American Mineralogist, Volume 77, pages 34–43, 1992

Mössbauer spectroscopy of tetrahedral Fe^{3+} in trioctahedral micas

D. G. Rancourt
Ottawa-Carleton Geoscience Centre and Ottawa-Carleton Institute for Physics, Department of Physics, University of Ottawa, Ottawa, Ontario K1N 6N5, Canada

M.-Z. Dang*
Ottawa-Carleton Institute for Physics, Department of Physics, University of Ottawa, Ottawa, Ontario K1N 6N5, Canada

A. E. Lalonde
Ottawa-Carleton Geoscience Centre, Department of Geology, University of Ottawa, Ottawa, Ontario K1N 6N5, Canada

Abstract

Six trioctahedral true micas are studied by Mössbauer spectroscopy and microprobe analysis. Three biotite samples, with a wide range of octahedral Fe^{3+}/Fe^{2+} ratios, chemical compositions that recalculate to full tetrahedral occupancies without requiring Fe^{3+}, and no trace of tetrahedral spectral components, are used for comparison. Both near end-member phlogopite and near end-member annite samples exhibit the same distinctive tetrahedral spectral feature as that of a reverse pleochroic phlogopite sample that is known (Hogarth et al., 1970) to contain $^{[4]}Fe^{3+}$. At room temperature, the latter spectral feature is a distinct shoulder occurring at $+0.41 \pm 0.02$ mm/s with respect to α-Fe—on the high-energy side of the mainly $^{[6]}Fe^{2+}$ peak at -0.1 mm/s. It arises from a relatively narrow distribution of quadrupole doublet splittings and can be used to assess unambiguously the presence of $^{[4]}Fe^{3+}$ from room-temperature Mössbauer spectra. It becomes significantly more distinctive at liquid N_2 temperatures—where it appears at $\sim +0.5$ mm/s.

All previous reports of $^{[4]}Fe^{3+}$ from Mössbauer spectra are reviewed and compared with our results. A pervasive mistake has been to assume that line positions for the hidden low-energy lines of tetrahedral doublets can be obtained reliably by fitting. When only the high-energy lines are considered, the true and brittle trioctahedral micas separate naturally into two fields that are consistent with the different interlayer charges of true and brittle micas. Another mistake is to believe in tetrahedral parameters lying outside these fields and corresponding to completely hidden doublets. In particular, such spectral contributions recently reported by Dyar (1990) are argued to be an artifact of improper analysis and interpretation.

Introduction

In natural and synthetic micas the biggest problem with Mössbauer spectroscopy arises from the superposition of different spectral lines. This makes discriminating the spectral components that result from different ions (Fe^{2+} and Fe^{3+}) or from ions in different crystallographic sites difficult, when not impossible. In this context, it is important to establish which information can be confidently obtained from the spectra and which arises as an artifact of improper analysis and overfitting.

The only separate spectral contributions that can be believed and used in quantitative measurements are those that give rise to distinct and resolved spectral features seen by visual inspection of high-quality spectra. Hidden spectral contributions buried under more intense lines—even such contributions that have reasonable or expected hyperfine parameters and that do not conflict with formula recalculations based on chemical analyses—should not be believed or used. In such situations, many other fits are statistically equivalent to the chosen one, and one can only conclude that the chosen model is not inconsistent with the data and that it cannot be distinguished from several other possible models.

The purpose of the present paper is to show that certain observed spectral features in the room-temperature and liquid-N_2 temperature Mössbauer spectra of trioctahedral micas unambiguously indicate the presence of $^{[4]}Fe^{3+}$ independently of any assumed line-shape fitting model. When these features are present, they can be used to estimate amounts of $^{[4]}Fe^{3+}$ that otherwise are missed by both the usual assignment method during formula recal-

* On leave from: Department of Physics, Hebei Normal University, Shi Jia Zhuang, Hebei, People's Republic of China.

0003–004X/92/0102–0034$02.00

TABLE 1. Sample descriptions

Sample	Description
MCL-PHL	Reverse pleochroic phlogopite mica from the McCloskey carbonatite, Quebec. Small flakes (~1–2 mm^2) separated from rock. Previously studied (Hogarth et al., 1970; Faye and Hogarth, 1969). This phlogopite sample has now been deposited in the mineral collection of the Royal Ontario Museum (sample no. M44527).
HEA-PHL	Phlogopite mica from the Headley mine near Old Chelsea, Quebec. Same single-crystal wafer as studied previously (Hargraves et al., 1990): approximately 4 cm × 5 cm × 335 μm.
ROM-ANN	Annite from Mont. St. Hilaire, Quebec. Specimen from the mineral collection of the Royal Ontario Museum, Toronto, Canada. Sample no. M42126. Magnetism previously studied (Rancourt et al., 1990). Single crystal ~1 cm × 1 cm × 350 μm.
HEP-BIO	Biotite from the Hepburn intrusive suite, Northwest Territories, Canada. Sample L341A (Lalonde, 1989). Very small flakes separated from rock. About 5 mg used in 0.5-in. diameter absorber.
BIS-BIO	Biotite from the Bishop intrusive suite, Northwest Territories, Canada. Sample L531 (Lalonde, 1989). Large flakes (~2 mm diameter) manually separated from rock and used to make a mosaic absorber.
MOC-BIO	Biotite from the Silver Crater mine near Bancroft, Ontario. Sample MOC2661 from the Canadian Museum of Nature, Mineral Sciences Division. Large single-crystal wafer: ~4 cm × 5 cm × 150 μm. This sample has been the subject of an extensive single-crystal and variable-temperature Mössbauer study (Rancourt et al., in preparation).

culation from microprobe analysis and not overly careful Mössbauer spectroscopy.

We compare our findings with all available Mössbauer data, including a study of a large number of specimens by Dyar (1990), and conclude that the usual analysis in terms of a $^{[4]}Fe^{3+}$ quadrupole doublet is misleading. We observe that the $^{[4]}Fe^{3+}$ hyperfine parameters of brittle trioctahedral micas are well resolved from those of true trioctahedral micas and that the spread of parameter values for trioctahedral micas is thereby not as wide as suggested (Dyar, 1987), in that it is probably composed of two separate fields. We argue that parameters falling outside these fields, especially those also corresponding to hidden lines only, are incorrect.

MATERIALS AND METHODS

The six mica samples used as Mössbauer absorbers in the present study are described in Table 1. Chemical analyses for all samples were obtained by microprobe analysis, in the same way as described elsewhere (Hargraves et al., 1990). The analyses and corresponding structural formulas are given in Table 2.

Transmission ^{57}Fe Mössbauer spectra were obtained, calibrated, and folded in the usual way (e.g., Hargraves et al., 1990) with a range of ± 4 mm/s. Folding is essential to produce a flat background with parameters that do not interact with those of the absorption lines when least-squares fitting. Thickness corrections (Rancourt, 1989) were not performed since accurate amounts of ionic populations were not required. All line positions and center shifts are given with respect to the center shift of a ^{57}Fe-enriched Fe foil at room temperature.

TABLE 2. Composition of trioctahedral micas

Sample*	MCL-PHL	HEA-PHL	ROM-ANN	HEP-BIO	BIS-BIO	MOC-BIO
No. of analyses**	6	4	4	4	3	4
SiO_2	42.44	39.51	34.06	34.24	36.54	38.65
TiO_2	0.12	1.25	1.00	2.93	3.13	2.22
Al_2O_3	9.72	14.30	8.91	19.16	14.64	11.09
FeO_{tot}	6.51	3.67	39.69	21.87	19.87	18.18
MnO	0.01	0.03	2.15	0.29	0.34	0.90
MgO	25.47	24.27	0.47	6.37	11.10	13.69
CaO	0	0.01	0	0.01	0.03	0
Na_2O	0.10	0.20	0.86	0.14	0.06	0.52
K_2O	10.58	9.55	8.56	9.26	9.76	9.45
F	4.45	4.19	0.45	0.63	3.59	3.87
Cl	0.01	0.03	0.02	0.32	0.69	0.08
O ≡ F, Cl	1.87	1.78	0.20	0.34	1.67	1.65
Total	97.54	95.23	95.97	94.88	98.08	97.00
Structural formulae based on 22 O atoms						
Si	6.121	5.728	5.882	5.333	5.554	5.940
$^{[4]}Al$	1.652	2.272	1.814	2.667	2.446	2.008
$^{[4]}Ti$	0.013	0	0.130	0	0	0.053
Σ_{tet}	7.786	8.000	7.826	8.000	8.000	8.000
$^{[6]}Al$	0	0.170	0	0.850	0.176	0
$^{[6]}Ti$	0	0.137	0	0.343	0.358	0.205
Fe^{2+}	0.785	0.445	5.732	2.848	2.527	2.337
Mn	0.002	0.004	0.315	0.038	0.044	0.118
Mg	5.478	5.245	0.120	1.478	2.514	3.136
Σ_{oct}	6.265	6.001	6.168	5.558	5.610	5.794
Ca	0.001	0.001	0	0.003	0.004	0
Na	0.028	0.058	0.289	0.044	0.017	0.156
K	1.948	1.765	1.886	1.839	1.893	1.853
Σ_{int}	1.977	1.824	2.175	1.885	1.914	2.009
F	2.029	1.922	0.246	0.308	0.330	1.878
Cl	0.004	0.007	0.007	0.084	0.023	0.020

* According to sample descriptions in Table 1.
** Number of analyses included in mean.

In fitting these spectra, as few Voigt lines as needed to give statistically ideal fits were used, without worrying about how the various Voigt lines are coupled into quadrupole doublets, etc. Voigt lines are better suited than Lorentzian lines for two reasons: (1) they are better able to handle spectral distortions from thickness effects (Rancourt, 1989), and (2) they are a natural choice when distributions of static hyperfine parameters (i.e., quadrupole splittings and center shifts in this application) are important (Rancourt and Ping, 1991). Distributions are important in mica and are the main reason that Lorentzian lines cannot be used (Hargraves et al., 1990).

RESULTS AND DISCUSSION

Recognizing $^{[4]}Fe^{3+}$

Room-temperature (22–24 °C) Mössbauer spectra of the six micas described in Tables 1 and 2 are shown in Figure 1. The fits corresponding to the parameters given in Table 3 are purposely not shown so that the spectral data can be scrutinized without interference or bias.

Samples HEP-BIO, BIS-BIO, and MOC-BIO have typical Mössbauer spectra of textured or single-crystal samples that do not contain any $^{[4]}Fe^{3+}$. Such spectra, in general, have three main absorption peaks at ~ -0.1, $+1.0$, and $+2.3$ mm/s. The peak at 2.3 mm/s is due only to high-energy lines of $^{[6]}Fe^{2+}$ quadrupole doublets. The peak at 1.0 mm/s is due only to high-energy lines of $^{[6]}Fe^{3+}$

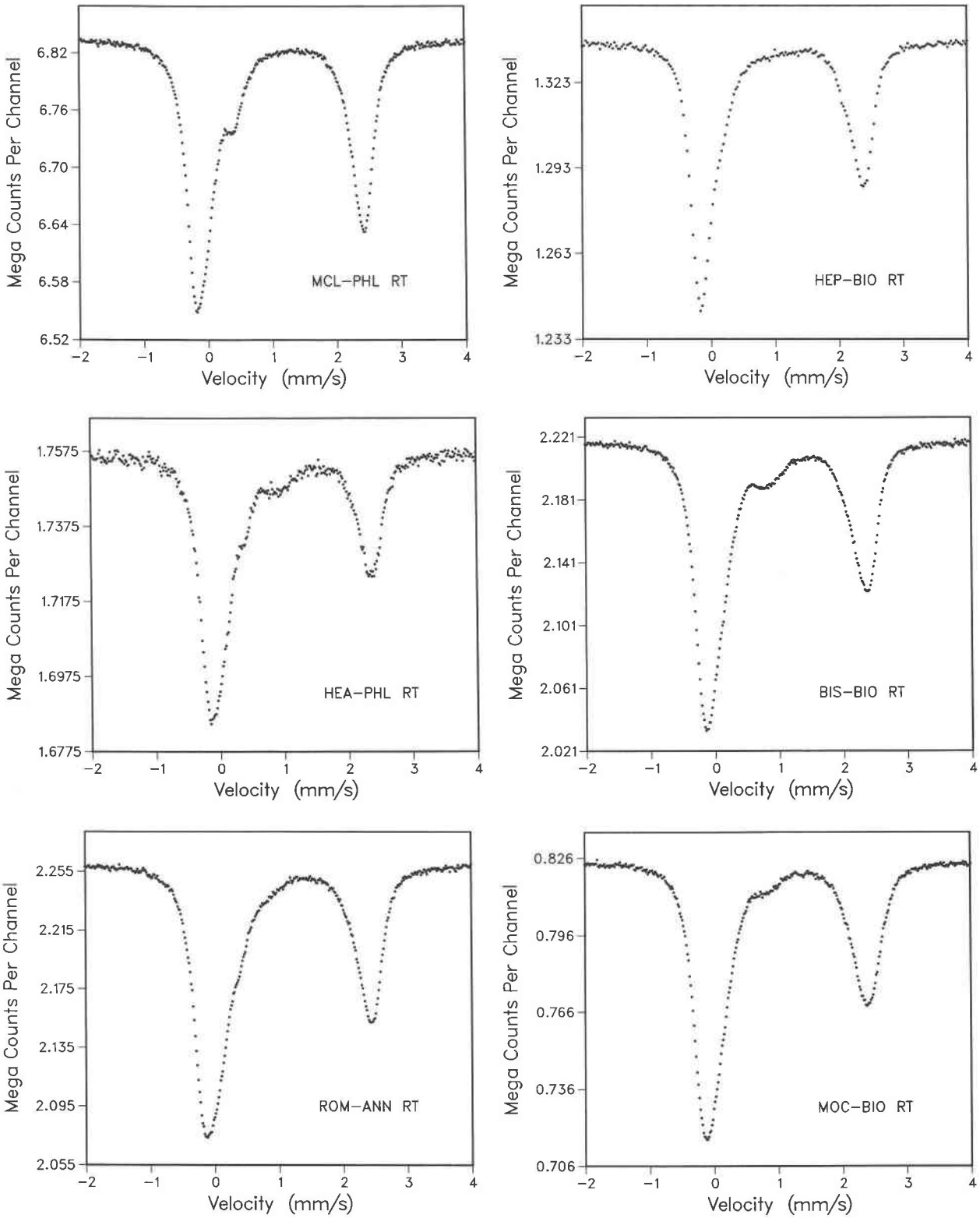

Fig. 1. Room-temperature (folded) Mössbauer spectra of the six natural micas (as labeled) described in Table 1.

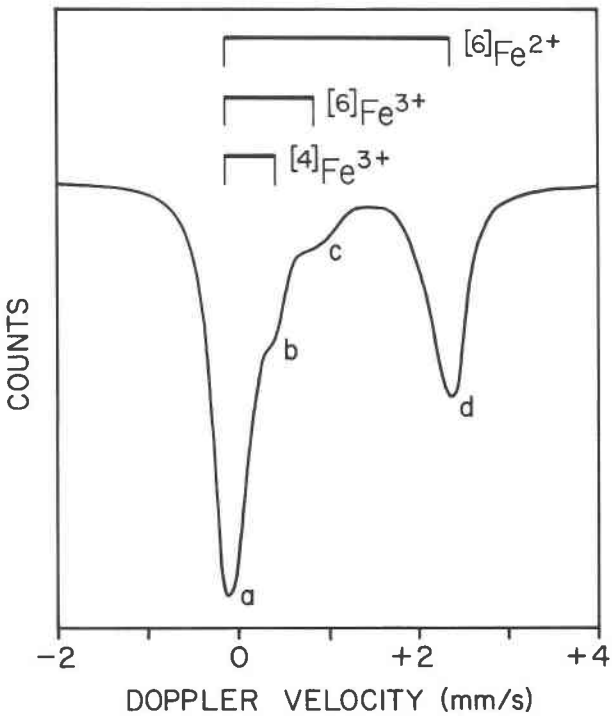

Fig. 2. Schematic representation of a room-temperature Mössbauer spectrum of a true trioctahedral mica containing $^{[6]}Fe^{2+}$, $^{[6]}Fe^{3+}$, and $^{[4]}Fe^{3+}$. Each type of ion gives rise to a distribution of quadrupole doublets. Each such family of doublets is represented by a "bar doublet" showing the approximate centroids of the high- and low-energy absorptions resulting from the distributions. Visible absorption line a is due to the low-energy contributions of all three ionic types; the three centroids are not actually at the same velocity as shown but usually cannot be resolved. Visible shoulder b is due to the high-energy doublet lines of the $^{[4]}Fe^{3+}$ contribution. Visible bump c is due to the high-energy doublet lines of the $^{[6]}Fe^{3+}$ contribution, and visible line d is due to the high-energy doublet lines of the $^{[6]}Fe^{2+}$ contribution. Shoulder b is the object of the present study.

quadrupole doublets. The peak at −0.1 mm/s, on the other hand, is due to the low-energy lines of quadrupole doublets corresponding to both the Fe^{2+} and the Fe^{3+} in octahedral sites. This is depicted schematically in Figure 2, where the tetrahedral doublet is also shown. From these assignments, it can be seen that sample HEP-BIO has a small octahedral Fe^{3+}/Fe^{2+} ratio, BIS-BIO has a relatively large ratio, and sample MOC-BIO has an intermediate value. The three spectra illustrate the range of octahedral Fe^{3+}/Fe^{2+} ratios encountered in natural biotite.

The spectrum for sample MCL-PHL has a prominent shoulder at ~0.4 mm/s that is believed to be the high-energy line of a quadrupole doublet (Figs. 1 and 2) corresponding to $^{[4]}Fe^{3+}$ (Hogarth et al., 1970). Since Fe-bearing richterite coexists with sample MCL-PHL in the rock, great care was taken to establish (1) that sample MCL-PHL was pure to better than 97 vol% and (2) that even a large amount of this amphibole could not cause the spectral feature at 0.4 mm/s.

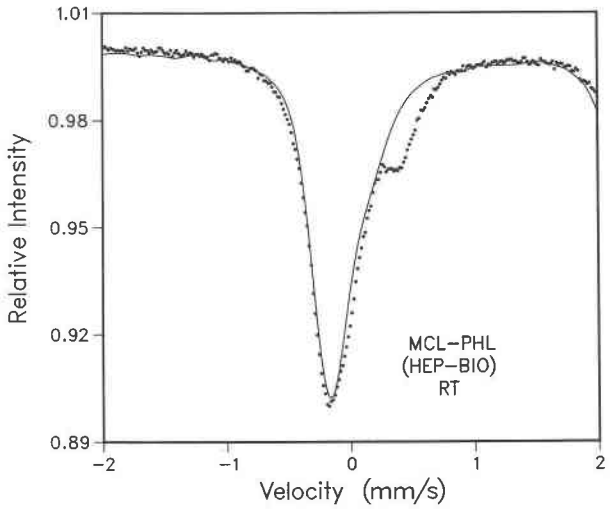

Fig. 3. Direct comparison (on expanded velocity scale) between spectra for samples MCL-PHL (data points) and HEP-BIO (solid line), showing the high-energy tetrahedral shoulder as a significant difference.

The shoulder at 0.4 mm/s in the spectrum for sample MCL-PHL is shown most clearly in an expanded and direct comparison with that of sample HEP-BIO (Fig. 3). It is too narrow and at too low an energy to correspond to $^{[6]}Fe^{3+}$, which usually gives absorption centered at 0.8–1.2 mm/s. Also, and most importantly, work done on a synthetic ferriphlogopite having all Fe in the form of $^{[4]}Fe^{3+}$ shows a quadrupole doublet with its high-energy line at ~0.4 mm/s (Annersten et al., 1971). We conclude that our feature is indeed due to $^{[4]}Fe^{3+}$ that must be present in sample MCL-PHL.

The same shoulder is also present in spectra of samples HEA-PHL and ROM-ANN (Fig. 1). That the spectrum of sample HEA-PHL indeed contains such a contribution is shown in expanded comparisons with spectra of sample MOC-BIO at both room temperature and liquid N_2 temperature (Fig. 4). The liquid N_2 temperature (actually 107 ± 2 K) spectra themselves are shown with Table 3 fits in Figure 5. At this temperature, the $^{[4]}Fe^{3+}$ shoulder has moved to ~0.5 mm/s (V_t in Table 3).

That samples HEA-PHL and ROM-ANN have $^{[4]}Fe^{3+}$ components is strongly supported by efforts to fit their spectra. Statistically ideal fits ($\chi^2_{red} \sim 1$ or less) are only obtained if the shoulder is allowed its own absorption line. Table 3 is a complete compilation of the Mössbauer-fit results that are discussed below.

Fitting the spectra

The main absorption line at −0.1 mm/s, in general, contains the low-energy quadrupole components of $^{[4]}Fe^{3+}$, $^{[6]}Fe^{3+}$, and $^{[6]}Fe^{2+}$ (line a in Fig. 2) and is modeled by Voigt lines 1 and 2 (Table 3). These two lines have no particular physical meaning. They mathematically model the effective absorption caused by all the true constituents of line a. The Fe^{3+} components are not resolved because

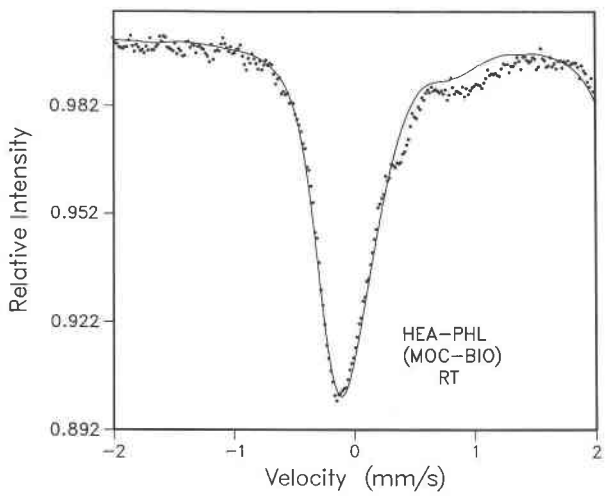

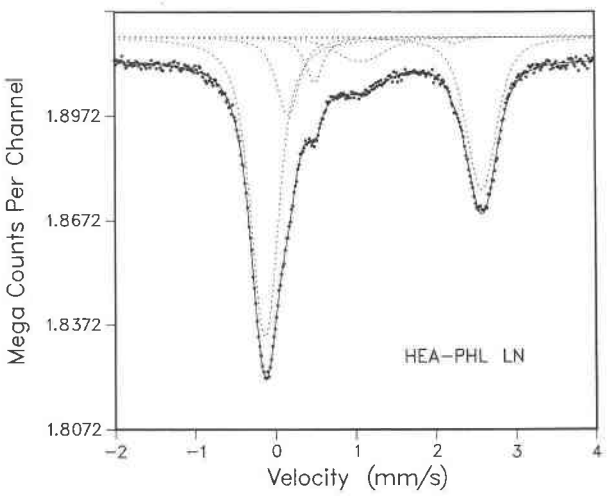

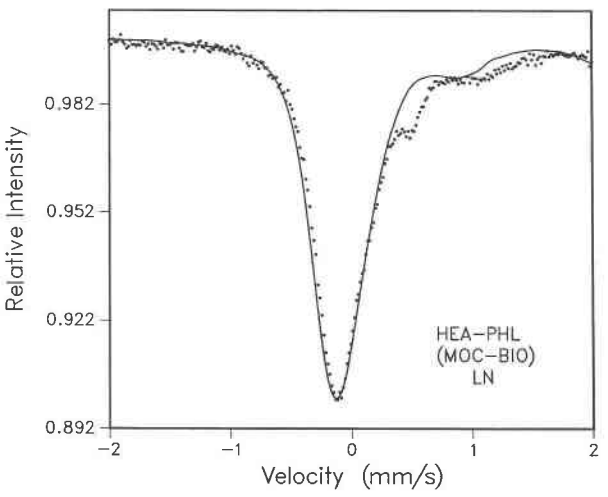

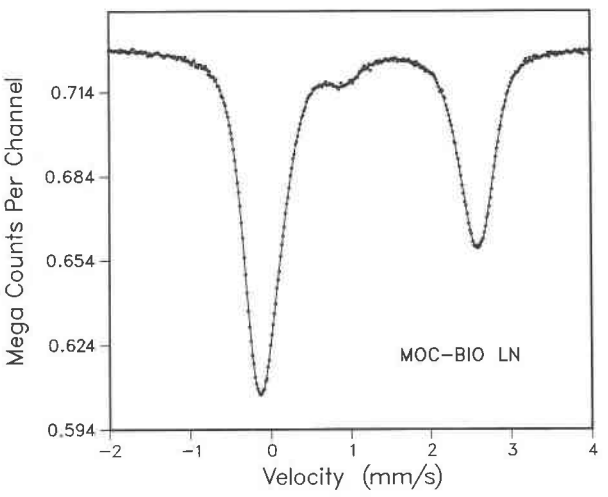

Fig. 4. Direct comparisons (on expanded velocity scales) of spectra for samples HEA-PHL (data points) and MOC-BIO (solid lines) at room temperature (RT) and liquid N_2 temperature (LN). At the lower temperature, the tetrahedral component is much more highly resolved and occurs at ~0.5 mm/s.

Fig. 5. Liquid N_2 temperature (actually 107 ± 2 K) Mössbauer spectra of the Headley phlogopite sample (HEA-PHL) and the MOC biotite sample (MOC-BIO). Solid lines correspond to the fits described in Table 3. Broken lines show the six individual Voigt components in the fit of the spectrum of sample HEA-PHL. These are shifted up to be more visible.

TABLE 3. Mössbauer fit results using either five or six Voigt lines*

Sample	T	σ_1	h_1	V_1	σ_2	h_2	V_2	σ_3	h_3	V_3	σ_4	h_4
MCL-PHL	RT	0.105	354.6	−0.159	0.277	155.5	0.191	0.185	61.4	2.235	0.084	230.1
HEA-PHL	RT	0.041	32.6	−0.196	0.144	81.0	−0.030	0.166	11.3	2.174	0.088	36.4
ROM-ANN	RT	0.066	140.2	−0.188	0.115	157.3	0.042	0.176	50.2	2.233	0.080	108.1
HEP-BIO	RT	0.082	104.6	−0.182	0.174	57.5	0.073	0.120	27.1	2.154	0.080	59.3
BIS-BIO	RT	0.072	118.4	−0.181	0.185	225.8	−0.011	0.180	73.1	2.167	0.091	99.6
MOC-BIO	RT	0.094	87.0	−0.171	0.183	117.0	0.033	0.237	36.3	2.253	0.130	66.7
HEA-PHL	LN	0.102	123.6	−0.133	0.063	27.4	0.163	0.000	2.2	2.246	0.120	67.1
MOC-BIO	LN	0.112	122.5	−0.178	0.174	103.5	0.022	0.183	26.9	2.435	0.135	98.1

* Here T is the absorber temperature (RT = 22–24 °C, LN = 107 ± 2 K), σ_i is the Gaussian width for the ith Voigt line (in mm/s), h_i is the Lorentzian height for the ith Voigt line (in kilocounts per channel), V_i is the ith Voigt line position (in mm/s with respect to metallic Fe at room temperature), γ is the Lorentzian FWHM (in mm/s) for all Voigt lines, and BG is the background level in megacounts per channel. Since common γ's are used, ratios of Voigt heights are equal to corresponding ratios of Voigt areas for a given spectrum.

** This parameter was frozen during fit.

they are relatively weak. The fact that two Voigts are needed for line a does not imply that Fe^{3+} components are present. For example, two Voigts are also needed for the purely octahedral Fe^{2+} absorption of line d (Fig. 2).

The absorption at +2.3 mm/s (line d in Fig. 2) is due only to the high-energy quadrupole doublet components of $^{[6]}Fe^{2+}$ and is modeled by Voigt lines 3 and 4. Here the need for two Voigt lines at different velocities implies an intrinsically asymmetric absorption line caused by a skewed distribution of Fe^{2+} elemental line positions. Such distributions are common and arise from the expected coupling between quadrupole splittings and center shifts (Rancourt and Ping, 1991).

Voigt line 5 (Table 3) is used to model the broad absorption band at 0.8–1.2 mm/s (line c in Fig. 2) arising from the high-energy quadrupole doublet components of $^{[6]}Fe^{3+}$. The Voigt line labeled "t" in Table 3 models the high-energy quadrupole doublet line arising from $^{[4]}Fe^{3+}$ (line b in Fig. 2) and is required to fit shoulders in the spectra of samples MCL-PHL, HEA-PHL, and ROM-ANN (Fig. 1).

Because of overlapping lines, it is impossible to obtain quantitative site populations from single-crystal, oriented, or textured samples unless enough is known about the hyperfine electric-field gradient magnitudes and directions (Rancourt, 1989; Hargraves et al., 1990). Given recent single-crystal work (Hargraves et al., 1990), $h_5/\Sigma\, h_i$ and $h_5/(h_3 + h_4)$, where h is the Lorentzian height for the particular Voigt line, can be used as lower and upper bounds, respectively, to the true ratio of total $^{[6]}Fe^{3+}$ to total spectal area. Also, given the negative sign of the Fe^{2+} electric field gradient ($e^2qQ < 0$), the lower bound is closer than the upper bound for highly textured or oriented samples, as in this study. Similarly, $h_t/\Sigma\, h_i$ and $h_t/(h_3 + h_4)$ are, respectively, taken to be lower and upper bounds to the true ratio of total $^{[4]}Fe^{3+}$ to total spectral area. These quantities (Table 3) allow us to conclude that (1) samples MCL-PHL, HEA-PHL, and ROM-ANN have comparable ratios of $^{[4]}Fe^{3+}$ to Fe_{tot} of ~5–10% and (2) that samples HEA-PHL and ROM-ANN have comparable amounts of tetrahedral and octahedral Fe^{3+}, whereas sample MCL-PHL probably has no $^{[6]}Fe^{3+}$.

The latter conclusions cannot easily be made based only on visual inspection of the spectra. Indeed, sample MCL-PHL seems to have a much larger $^{[4]}Fe^{3+}$ to Fe_{tot} ratio than any other sample, and sample HEA-PHL seems to have much more $^{[6]}Fe^{3+}$ than $^{[4]}Fe^{3+}$. This illustrates the difficulties related to strongly overlapping lines. The $^{[4]}Fe^{3+}$ shoulder in the spectrum of sample MCL-PHL is more prominent visually only because the −0.1 mm/s line is more narrow.

In conclusion, the fit results (Table 3) show a $^{[4]}Fe^{3+}$ shoulder or line at 0.41 ± 0.02 mm/s in the three samples showing such a contribution. This is significant in that almost ideal end-members phlogopite and annite are included, suggesting that any trioctahedral true mica containing $^{[4]}Fe^{3+}$ should have a room-temperature contribution at this well-defined velocity.

Another result from the fits is that the $^{[4]}Fe^{3+}$ distribution of quadrupole splittings is very narrow compared with the octahedral sites. In fact, our results indicate an absence of distribution broadening ($\sigma_t \approx 0$ with a normal $\gamma \sim 0.2$ mm/s). This is consistent with the much smaller local-environment viability in tetrahedral sites compared with octahedral sites. On tetrahedral sites the near neighbors are four O atoms, whereas in octahedral sites they are four O atoms and 2 OH^- groups in either *cis* or *trans* arrangements and with defects such as H vacancies and OH^- being replaced by F^- or Cl^-. The further neighbor environments are also more variable in the octahedral sites, with a great variety of possible octahedral cations compared with almost only Si^{4+}, Al^{3+}, and Fe^{3+} in the tetrahedral sites.

This sharpness makes the $^{[4]}Fe^{3+}$ shoulder at 0.41 mm/s more observable than it otherwise would be. It makes the high-energy tetrahedral line distinct and recognizable despite its overlap with the absorption at ~−0.1 mm/s. Excellent statistics (e.g., $S/N \geq 50$) and a high channelwise resolution (e.g., channel-width ≤ 0.015 mm/s) are nonetheless desirable if the presence of $^{[4]}Fe^{3+}$ is to be ascertained unambiguously.

Finally, we comment on "fit quality." The reduced chi squared (χ^2_{red}) values are given in Table 3. The fits to the room temperature spectra (Table 3 but not shown) were

Table 3—*Continued*

V_4	σ_5	h_5	V_5	σ_t	h_t	V_t	γ	BG	χ^2_{red}	$h_5/\Sigma\, h_i$	$h_5/(h_3 + h_4)$	$h_t/\Sigma\, h_i$	$h_t/(h_3 + h_4)$
2.425	—	—	—	0.000	26.9	0.426	0.241	6.834	1.22	—	—	0.033	0.092
2.376	0.205	13.5	0.949	0.000	10.6	0.397	0.262	1.757	0.52	0.073	0.283	0.057	0.223
2.450	0.278	28.5	0.740	0.052	33.7	0.391	0.280	2.260	0.59	0.055	0.180	0.065	0.213
2.403	0.388	9.8	0.84**	—	—	—	0.214	1.337	0.27	0.038	0.114	—	—
2.386	0.249	51.9	0.841	—	—	—	0.220	2.218	0.57	0.091	0.300	—	—
2.411	0.192	14.3	0.830	—	—	—	0.236	0.825	0.49	0.045	0.139	—	—
2.581	0.254	16.4	1.067	0.000	13.5	0.495	0.261	1.913	0.49	0.066	0.236	0.054	0.195
2.610	0.185	17.8	0.906	—	—	—	0.237	0.730	0.53	0.048	0.142	—	—

TABLE 4. Previously reported $^{[4]}Fe^{3+}$ in room temperature spectra of micas

Dyar's no.	% tet. layer	tet.3+/ total	A_{tet}/A_{tot}	δ_t	Δ_t	L_t	H_t	oct.2+	oct.3+	Reference
2P	4.0	0.40	0.40	0.20	0.52	−0.06	0.46	yes	no	Shinno and Suwa (1981)
3P	3.5	0.42	0.42	0.24	0.47	−0.005	0.475	yes	no	Shinno and Suwa (1981)
4L	0.3	0.05	0.04	0.25	0.35	+0.075	0.425	yes	no	Levillain et al. (1977)
6P	2.5	0.50	—	0.26	0.62	−0.05	0.57	no	yes	Ishida and Hirowatari (1980)
7P	5.0	0.50	0.50	0.15	0.63	−0.165	0.465	yes	no	Ishida and Hirowatari (1980)
33B	3.0	0.39	0.29	0.26	0.45	+0.035	0.485	yes	no	Sanz et al. (1978)
54P	3.6	0.37	0.26	0.19	0.44	−0.03	0.41	yes	no	Hogarth et al. (1970)
55P	0.9	0.09	—	0.21	0.44	−0.01	0.43	yes	yes	Hogarth et al. (1970)
59C	1.3	0.50	0.54	0.27	0.62	−0.04	0.58	yes	yes	Annersten and Olesch (1978)
60C	1.5	0.55	0.55	0.24	0.68	−0.10	0.58	yes	yes	Annersten and Olesch (1978)
62C	3.4	0.77	0.76	0.26	0.65	−0.065	0.585	yes	no	Annersten and Olesch (1978)
63C	6.5	0.87	0.87	0.24	0.80	−0.16	0.64	no	yes	Annersten and Olesch (1978)
78A	4.5	0.08	0.03	0.20	0.37	+0.015	0.385	yes	yes	Dyar and Burns (1986)
79A	10.6	0.21	0.16	0.19	0.39	−0.005	0.385	yes	yes	Dyar and Burns (1986)
80A	16.4	0.23	0.20	0.21	0.40	+0.01	0.41	yes	yes	Dyar and Burns (1986)
81A	13.8	0.18	0.18	0.20	0.45	−0.025	0.425	yes	yes	Dyar and Burns (1986)
82P	5.9	0.38	0.62	0.19	0.56	−0.09	0.47	yes	no	Dyar and Burns (1986)
87P	—	—	1.00	0.17	0.50	−0.08	0.42	no	no	Annersten et al. (1971)
88P	—	—	—	0.19	0.57	−0.095	0.475	yes	no	Huggins (1976)
133B	—	—	—	0.13	0.54	−0.14	0.40	yes	yes	Pollak and Bruyneel (1974)
145B	—	—	—	0.32	0.58	+0.03	0.61	yes	no	Vertes et al. (1981)

of the same visual and statistical quality as the fits (Fig. 5) to the liquid N_2 temperature spectra. The somewhat larger χ^2_{red} value for sample MCL-PHL at room temperature may be due to a very small amount of $^{[6]}Fe^{3+}$. We are investigating this possibility in a detailed study of sample MCL-PHL (Rancourt et al., in preparation).

Comparing the Mössbauer results to formula recalculations

Our Mössbauer analysis shows that samples MCL-PHL, HEA-PHL, and ROM-ANN have ~5–10% of their total Fe as $^{[4]}Fe^{3+}$, whereas the biotite samples HEP-BIO, BIS-BIO, and MOC-BIO have no $^{[4]}Fe^{3+}$.

By comparison, our formula recalculations from the microprobe analyses, based on all Fe as FeO, strongly indicate $^{[4]}Fe^{3+}$ only in samples MCL-PHL and ROM-ANN, which have the largest total amounts. These two samples have octahedral sums significantly larger than 6 and tetrahedral sums significantly smaller than 8 (Table 2), as is expected from ignoring $^{[4]}Fe^{3+}$. The three biotite samples that have no $^{[4]}Fe^{3+}$ detectable in their Mössbauer spectra have tetrahedral sums of 8 and octahedral sums that are significantly smaller than 6. The latter is usual and probably due to octahedral vacancies and octahedral ions that were not analyzed.

Sample HEA-PHL has $\Sigma_{oct} = 6.0$ and $\Sigma_{tet} = 8.0$. This sample does not have enough $^{[4]}Fe^{3+}$ to make its presence obvious in the recalculation; however, its ideal octahedral sum is, in hindsight, suspect and might be used as an indicator of $^{[4]}Fe^{3+}$. This shows that, whereas the presence of $^{[6]}Fe^{3+}$ is usually impossible to ascertain from formula recalculations, the presence of $^{[4]}Fe^{3+}$ is more easily recognized.

On the other hand, in room-temperature Mössbauer spectra, $^{[4]}Fe^{3+}$ can more easily be missed than $^{[6]}Fe^{3+}$. For example, Hargraves et al. (1990) studied the same single-crystal wafer of sample HEA-PHL and did not recognize the tetrahedral shoulder. This is due to small experimental differences (better MCS electronics and smaller channel width in the present study) and to not knowing what to look for. The present paper shows exactly what to look for. Compare the spectrum for sample HEA-PHL in Figure 1 to Figures 2 and 4 of Hargraves et al. This suggests that true $^{[4]}Fe^{3+}$ may have been missed frequently in past studies.

Comparison with previous work

Dyar (1987) has reviewed the room-temperature Mössbauer work on trioctahedral micas. Of the 130 samples reported by Dyar, 31 samples are claimed by the respective authors to show a distinct spectral component due to $^{[4]}Fe^{3+}$.

On close examination, we find that in at least five of the latter samples (samples 1B, 9B, 21B, 77B, and 119B in Dyar's list) the $^{[4]}Fe^{3+}$ component actually corresponds to $^{[6]}Fe$. Also, a group of spectra from samples studied by Manapov and Sitdikov (1974) and Manapov and Krinari (1976) (samples 48B, 49B, 51B, 128B, and 129B) seem to have a systematic calibration error in absolute velocity with respect to metallic Fe (or in any case are of very poor quality) and will therefore be omitted from further consideration.

Information concerning the remaining 21 samples is given in Table 4. Here each sample is labeled with Dyar's sample number that contains a letter indicating the type of mica as classified by the original authors (P = phlogopite, B = biotite, A = annite, C = clintonite, and L = lepidolite). The other quantities in Table 4 are defined as follows: % tet. layer is the claimed percentage of the tetrahedral sites that contain Fe^{3+}; tet.3+/total is the claimed

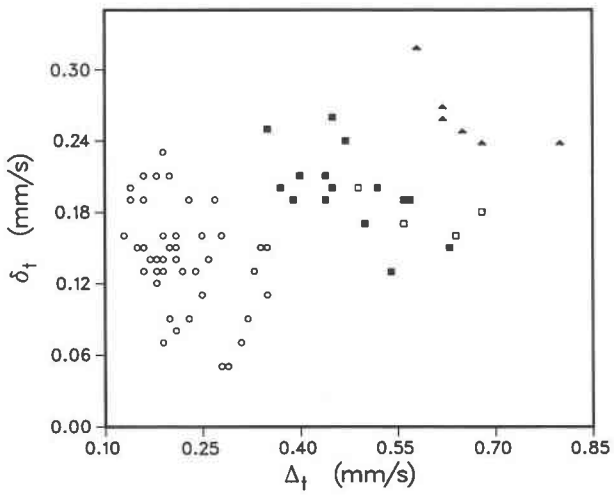

Fig. 6. Previously reported values of room-temperature center shifts (with respect to α-Fe) vs. quadrupole splittings of supposed tetrahedral doublets in trioctahedral micas. Such δ-Δ plots are often used but do not justly reflect the large uncertainties related to hidden lines. Points in our brittle mica field are represented as filled triangles. Those in our true mica field are represented by filled squares. The points taken from Dyar's recent study (Dyar, 1990) are represented by open symbols. Not all of Dyar's points are visible because of overlap. The filled symbol parameters are given in Table 4.

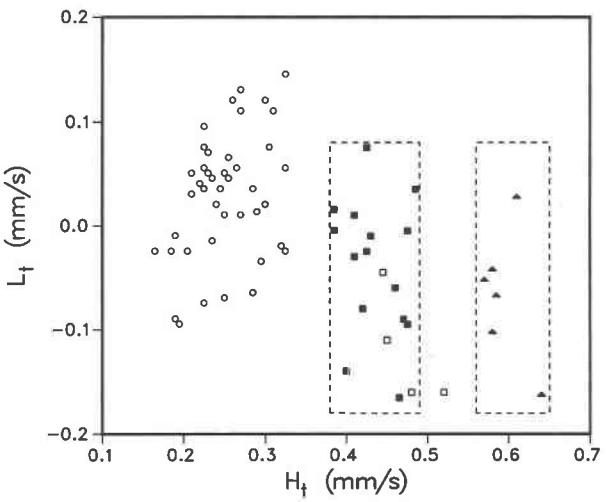

Fig. 7. L_t-H_t plot, as an alternative to the δ_t-Δ_t plot (Fig. 6). Here L_t is the position of the low-energy tetrahedral line ($L_t = \delta_t - \Delta_t/2$) and H_t is the position of the high energy component ($H_t = \delta_t + \Delta_t/2$). H_t is well separated into true and brittle mica fields. The symbols have the same meanings as in Figure 6. The new "field," at $H_t \sim 0.15$–0.35 mm/s, that appears on plotting Dyar's data (Dyar, 1990) is most probably not real, as explained in the text.

fraction of the Fe_{tot} that is $^{[4]}Fe^{3+}$ (from chemical analysis or combined chemical analysis and Mössbauer); A_{tet}/A_{tot} is the ratio of the spectral area of the $^{[4]}Fe^{3+}$ quadrupole doublet to the total Mössbauer spectral area; δ_t and Δ_t are, respectively, the center shift with respect to metallic Fe and the quadrupole splitting of the assumed $^{[4]}Fe^{3+}$ quadrupole doublet; L_t and H_t are, respectively, the low- and high-energy line positions of the quadrupole doublets corresponding to δ_t and Δ_t (i.e., $L_t = \delta_t - \Delta_t/2$ and $H_t = \delta_t + \Delta_t/2$); oct.2+ indicates whether the spectrum showed $^{[6]}Fe^{2+}$; and oct.3+ indicates whether the spectrum showed any $^{[6]}Fe^{3+}$.

Whereas a surprising diversity of (δ_t, Δ_t) values is reported (Table 4 and Fig. 6), much of this diversity is seen to be an artifact when the corresponding line positions themselves (L_t and H_t) are examined (Fig. 7). This is because, most often, only H_t corresponds to a visible spectral feature (line or shoulder), whereas L_t corresponds to a contribution that is hidden under the strong $^{[6]}Fe^{2+}$ and $^{[6]}Fe^{3+}$ absorption at ~ -0.1 mm/s. Indeed, H_t is found to be meaningful, whereas L_t has a broad range of values from approximately -0.2 to $+0.1$ mm/s.

This is seen in Figure 7, which shows two narrow fields of H_t values: one at 0.38–0.49 mm/s corresponding to trioctahedral true micas in agreement with our results ($H_t = V_t = 0.41 \pm 0.02$ mm/s; Table 3) and one at 0.56–0.65 mm/s corresponding to trioctahedral brittle micas (clintonite). The latter field contains all the clintonite samples reported in Dyar's review (samples 59C, 60C, 62C, and 63C) and two other samples identified by the original authors as true micas (6P and 145B). In a δ-Δ plot (Fig. 6), the true and brittle fields have widely overlapping values of both δ_t and Δ_t.

In addition, on examining Table 4 and Figure 7, we find that other trends also seem to exist: (1) annite seems to have lower H_t values than phlogopites, especially phlogopite that does not contain $^{[6]}Fe^{3+}$, and (2) biotite containing $^{[4]}Fe^{3+}$ seems to be relatively rare compared with annite and phlogopite. Both the above points are supported by the present study of six micas.

Figures 6 and 7 also show points (open symbols) of the recent work by Dyar (1990) involving 52 biotite samples from metapelites, all reported to contain $^{[4]}Fe^{3+}$. Only four samples are within our true mica field (samples O-K-15, O-K-53, O-C-26, and OB16); one is not visible because of overlap of points. One sample (Ra-d37-66) lies directly between our true and brittle mica fields. The spectra for the latter samples are not shown by Dyar. Only one spectrum is shown (sample O-L-10), which in our opinion has no detectable $^{[4]}Fe^{3+}$ since it lacks the characteristic shoulder at $\sim$0.4 mm/s or higher.

The tetrahedral doublet in this spectrum (O-L-10) is seen as consisting of two weak and highly overlapping lines that are completely buried in the main absorption line centered at ~ -0.1 mm/s. They do not give rise to a noticeable spectral feature that might be used as evidence for their existence.

In all, 47 of Dyar's (1990) samples have tetrahedral doublet parameters similar to those of O-L-10 and presumably have similarly hidden lines. This group of samples gives rise to a new field (Figs. 6 and 7, open circles) that is as far removed from that of the true micas as is

that of the brittle micas—only in the opposite direction. In our opinion, this new field is an artifact of overfitting and is not real.

Dyar (1990) claims that the new tetrahedral parameters are in agreement with previous work; however, they are clearly and systematically different from all previously reported values (Figs. 6 and 7). Whereas quadrupole splittings of ~0.40–0.55 mm/s have mainly been reported for trioctahedral true micas, Dyar's biotite samples are reported to have an average of $\langle\Delta_t\rangle = 0.25(12)$ mm/s (Fig. 6; Dyar, 1990). Such a difference is difficult to understand. The quadrupole splitting of an Fe^{3+} ion arises from the lattice point-charge contribution only, and Dyar should explain how the latter can be so small in her biotite samples, compared to all other trioctahedral micas.

In addition, Dyar (1990) describes how, given present understanding of the crystal chemistry of micas, her biotite samples should not contain $^{[4]}Fe^{3+}$. This unusual $^{[4]}Fe^{3+}$, whose presence is not directly detected in the spectra (unlike the $^{[6]}Fe^{2+}$ and $^{[6]}Fe^{3+}$), was not corroborated by an independent measurement. Also, a distinction is not made between the 47 samples that have the unusual parameters and the other five whose parameters are stepwise different and more usual.

Dyar (1990) has fitted each spectrum in several different ways ("In some samples 30–50 different models were tested . . .") and has found a group of fits that give a consistent interpretation in the sense that the different lines are always present in about the same positions. This is, in our experience, no reason to believe in weak and hidden lines, especially when such lines are inconsistent with present knowledge and thereby require an ad hoc and specialized explanation.

Dyar's new tetrahedral parameters are probably an artifact of improper analysis and interpretation. A plausible mechanism for this artifact is as follows. Slight absorber texture, as is virtually impossible to avoid with micas, will shift intensity from the high-energy $^{[6]}Fe^{2+}$ line to the low-energy $^{[6]}Fe^{2+}$ line, thereby requiring extra intensity in a broad neighborhood of ~ -0.1 mm/s when symmetric quadrupole doublet models are used (as was the case). This error will occur in about the same way in similar samples and will lead to false lines in about the same positions and of about the same relative intensities. This is what was observed by Dyar, with a tetrahedral doublet corresponding to a nearly constant fraction (~8%) of the Fe_{tot}. When possible texture effects, thickness effects, and non-Lorentzian line shapes resulting from quadrupole splitting distributions are all ignored, then such small and systematic false spectral contributions should be expected.

Conclusions

The $^{[4]}Fe^{3+}$ in true trioctahedral micas gives a room-temperature quadrupole doublet having center shift $\delta_t \approx 0.17$ mm/s (with respect to α-Fe) and quadrupole splitting $\Delta_t \approx 0.50$ mm/s (Annersten et al., 1971). In natural samples, this leads to a low-energy line whose position ($L_t = \delta_t - \Delta_t/2 \approx -0.08$ mm/s) is such that it is completely buried under the large absorption line mainly caused by $^{[6]}Fe^{2+}$ and centered at ~ -0.1 mm/s (Fig. 2). Consequently, in most cases reliable information cannot be obtained concerning the low-energy tetrahedral line except that it is hidden, i.e., it lies somewhere between -0.2 and $+0.1$ mm/s (Fig. 7). On the other hand, the high-energy tetrahedral line has a position ($H_t = \delta_t + \Delta_t/2 \approx 0.42$ mm/s) that potentially makes it resolvable from the $^{[6]}Fe^{2+}$ and $^{[6]}Fe^{3+}$ lines. The H_t line is indeed resolvable (largely thanks to its relatively small width) and can be used to recognize unambiguously the presence of (and to quantify the amounts of) $^{[4]}Fe^{3+}$ in natural samples.

Brittle trioctahedral micas have $H_t \approx 0.6$ mm/s (Fig. 7) such that, assuming about the same center shift as in true trioctahedral micas ($\delta_t \approx 0.2$ mm/s), we expect $\Delta_t \approx 0.8$ mm/s and $L_t \approx -0.2$ mm/s—again making the low energy line unobservable in most cases. The larger Δ_t value for brittle micas is consistent with the larger interlayer charge.

In comparing different natural samples, only H_t values are dependable; separate δ_t and Δ_t values are not since these are uncertain to the extent that L_t is uncertain. Two fields of H_t values seem to exist: a true trioctahedral mica field at 0.38–0.49 mm/s and a brittle trioctahedral mica field at 0.56–0.65 mm/s. Our samples, including near end-members phlogopite and annite, gave $H_t = 0.39$–0.43 mm/s. It is difficult to assess how much of the field widths are actually due to lab-to-lab calibration differences.

Supposed tetrahedral contributions having $H_t > 0.7$ mm/s are suspect because of the known $^{[6]}Fe^{3+}$ line at 0.8–1.2 mm/s. They are most probably incorrectly identified contributions. We do not expect that the tetrahedral sites can produce such large quadrupole splittings.

Supposed tetrahedral contributions having $H_t < 0.35$ mm/s, such as recently reported by Dyar (1990) for biotite samples, are also suspect because (1) in this case, both tetrahedral doublet lines are essentially hidden by the broad and mainly $^{[6]}Fe^{2+}$ absorption at ~ -0.1 mm/s and (2) such values are significantly outside the above-described fields that are based on several samples in which the presence of $^{[4]}Fe^{3+}$ is often corroborated by independent observations such as the occurrence of reverse pleochroism. We have shown that Dyar's new tetrahedral parameters are most likely an artifact of improper analysis and interpretation.

We stress that it is important to rely on visible spectral features (the sharp room temperature shoulder at ~0.41 mm/s, e.g., Figs. 3 and 4), rather than numerical results from multiline fits using arbitrary constraints and assumptions, to identify positively the presence or absence of $^{[4]}Fe^{3+}$. The visible shoulder can be enhanced by such aids as obtaining spectra at low temperatures, using the smallest practical channel width (or region of interest scans), and acquiring the best possible statistics.

Acknowledgments

We thank G. Robinson of the Canadian Museum of Nature for supplying specimen MOC2661 and J.A. Mandarino of the Royal Ontario Museum for specimen M42126. We thank D.D. Hogarth for help in locating

the McCloskey sample. Financial support from the Natural Sciences and Engineering Research Council of Canada to D.G.R. and A.E.L. is gratefully acknowledged.

References cited

Annersten, H., and Olesch, M. (1978) Distribution of ferrous and ferric iron in clintonite and the Mössbauer characteristics of ferric iron in tetrahedral coordination. Canadian Mineralogist, 16, 199–203.

Annersten, H., Devanarayanan, S., Häggström, L., and Wäppling, R. (1971) Mössbauer study of synthetic ferriphlogopite $KMg_3Fe^{3+}Si_3O_{10}(OH)_2$. Physica Status Solidi B, 48, K137–K138.

Dyar, M.D. (1987) A review of Mössbauer data on trioctahedral micas: Evidence for tetrahedral Fe^{3+} and cation ordering. American Mineralogist, 72, 102–112.

——— (1990) Mössbauer spectra of biotite from metapelites. American Mineralogist, 75, 656–666.

Dyar, M.D., and Burns, R.G. (1986) Mössbauer spectral study of ferruginous one-layer trioctahedral micas. American Mineralogist, 71, 955–965.

Faye, G.H., and Hogarth, D.D. (1969) On the origin of 'reverse pleochroism' of a phlogopite. Canadian Mineralogist, 10, 25–34.

Hargraves, P., Rancourt, D.G., and Lalonde, A.E. (1990) Single-crystal Mössbauer study of phlogopite mica. Canadian Journal of Physics, 68, 128–144.

Hogarth, D.D., Brown, F.F., and Pritchard, A.M. (1970) Biabsorption, Mössbauer spectra, and chemical investigation of five phlogopite samples from Québec. Canadian Mineralogist, 10, 710–722.

Huggins, F.E. (1976) Mössbauer studies of iron minerals under pressures of up to 200 kbars. In R.G.J. Sterns, Ed. The physics and chemistry of minerals and rocks, p. 613–640. Wiley, New York.

Ishida, K., and Hirowatari, F. (1980) On the chemical composition and Mössbauer spectra of manganoan phlogopite with reverse pleochroism. Kobutsugaku Zasshi, 14 (Tokubet sugo 3), 54–61.

Lalonde, A.E. (1989) Hepburn intrusive suite: Peraluminous plutonism within a closing back-arc basin, Wopmay orogen, Canada. Geology, 17, 261–264.

Levillain, C., Maurel, P., and Menil, F. (1977) Localization du fer, par voie chimique et par spectrométrie Mössbauer, dans la lépidolite du granite de Beauvoir (Massif central français). Bulletin de la Société Française de Minéralogie et de Cristallographie, 100, 137–142.

Manapov, R.A., and Krinari, G.A. (1976) Gamma-resonance spectroscopy of layer silicates and some problems of their crystal chemistry. In V.M. Vinokurov, Ed., Fiz Svoistva Miner Gorn Porod, p. 110–122. Izdanja Kazan Universiteta, Kazan, USSR.

Manapov, R.A., and Sitdikov, B.S. (1974) Metamorphic rocks of the Precambrian basement in the Tatar Dome. Geochemistry International, 11, 976–980.

Pollak, H., and Bruyneel, W. (1974) Saut d'électrons et le rapport Fe^{2+}/Fe^{3+} dans deux silicates. Journal de Physique, Colloque, 35, C6-571–C6-574.

Rancourt, D.G. (1989) Accurate site populations from Mössbauer spectroscopy. Nuclear Instruments and Methods in Physics Research, B44, 199–210.

Rancourt, D.G., and Ping, J.Y. (1991) Voigt-based methods for arbitrary-shape static hyperfine parameter distributions in Mössbauer spectroscopy. Nuclear Instruments and Methods in Physics Research, B58, 85–97.

Rancourt, D.G., Lamarche, G., Tume, P., Lalonde, A.E., Biensan, P., and Flandrois, S. (1990) Dipole-dipole interactions as source of spin glass behaviour in random ferromagnetic-layer compounds. Canadian Journal of Physics, 68, 1134–1137.

Sanz, J., Meyers, J., Vielvoye, L., and Stone, W.E.E. (1978) The location and content of iron in natural biotites and phlogopites: A comparison of several methods. Clay Minerals, 13, 45–52.

Shinno, I., and Suwa, K. (1981) Mössbauer spectrum and polytype of phlogopite with reverse pleochroism. Sixth Preliminary Report of African Studies, p. 151–157. Nagoya University, Nagoya, Japan.

Vertes, A., Jonas, K., Czako-Nagy, I., and Nemecz, E. (1981) A combined application of Mössbauer spectroscopy and chemical transformation for chemical analysis. Radiochemical and Radioanalytical Letters, 48, 93–100.

Manuscript received October 4, 1990
Manuscript accepted August 1, 1991